Progress In Electromagnetics Research B, Vol. 22, 39–52, 2010

A COMPARATIVE STUDY OF HIGH BIREFRINGENCE AND LOW CONFINEMENT LOSS PHOTONIC CRYSTAL FIBER EMPLOYING ELLIPTICAL AIR HOLES IN FIBER CLADDING WITH TETRAGONAL LATTICE

Y.-F. Chau, C.-Y. Liu, and H.-H. Yeh

Department of Electronic Engineering
Ching Yun University
Jung-Li 320, Taiwan, R.O.C.

D. P. Tsai

Department of Physics
National Taiwan University
Taipei 10617, Taiwan, R.O.C.

Abstract—We numerically compare the mode birefringence and confinement loss with four patterns (case A–D) of index-guiding photonic crystal fibers (PCF) using the finite element method. These PCFs are composed of a solid silica core surrounded by different sizes of elliptical air holes and a cladding which consist of the same elliptical air holes in fiber cladding with tetragonal lattice. The maximal modal birefringence and lowest confinement loss of our proposed case A structure at the excitation wavelength of $\lambda = 1550\,\text{nm}$ can be achieved at a magnitude of 5.3×10^{-2} (which is the highest value to our knowledge) and less than $0.051\,\text{dB/km}$ (an acceptable value less than $0.1\,\text{dB/km}$) with only four rings of air holes in fiber cladding, respectively. The merit of our designed PCFs is that the birefringence and confinement loss can be easily controlled by turning the pitch (hole to hole spacing) of elliptical air holes in PCF cladding.

Corresponding author: Y.-F. Chau (yfc01@cyu.edu.tw).

1. INTRODUCTION

Photonic crystal fibers (PCFs) have attracted a lot of research attention due to many possibilities and promising applications in communication and sensing [1, 2]. Based on the design flexibility and the large index contrast, high birefringence can be easily realized in PCFs. The birefribgence of index guiding PCFs has a magnitude of the order of 10^{-3}, which is 1 order of magnitude higher than the conventional fiber (the order of 10^{-4}). Symmetry in PCFs implies the existence of doubly-degenerate pairs of modes, that share the same propagation constant (β) and free-space wavelength (λ), so they must be degenerate. As a result, the observation of birefringence must be a result of asymmetry in the structure. These perturbations couple the modes that propagate at slightly different phase velocities, with the consequence that the polarization of light becomes unpredictable after a short propagation. To overcome this drawback, it is highly desirable to generate a large birefringence (as high as possible) with a low confinement loss (as low as possible), and to avoid significant perturbations in the cladding modes to cope with recent challenges and demands in fiber optic polarization control.

To our knowledge, there are many methods to realized high birefringence in index-guding PCFs by making the structure of the PCF asymmetric. One effective way is to replace circular air holes in the cladding with elliptical ones [3]. For the PCFs of this category, high birefringence is achieved when the bulk of the mode energy is in the fiber cladding; thus, the high birefringence is often accompanied with poor energy confinement [4–6]. Based on our previous works [7], in this paper, we numerically investigate a novel high-birefringence and low confinement loss index-guiding PCF using the finite element method (FEM). Four patterns of PCFs are investigated to compare. The origin of the birefringence is discussed in detail and its dependence on the structural parameters is analyzed. Furthermore, we discuss the influence of the rings of air holes on birefringence and confinement loss. Finally, we will show that such a design is able to offer a perfect solution to the tradeoff between the high birefringence and the confinement loss in elliptical-hole with tetragonal lattice PCFs.

2. SIMULATION MODELS, METHOD, RESULTS AND DISCUSSION

The numerical method used in this study is FEM [8]. The fiber cross section representation is very accurate as the domain is divided into sub-domains with triangular or quadrilateral shape where any

refractive index profiles can be properly represented. Applying the variational FEM procedure to the curl-curl equation for magnetic field H, one obtains an eigenvalue equation $([P] - \beta^2[Q])\{H\} = 0$, where $\{H\}$ is the global magnetic field vector, β is the propagation constant, and $[P]$ and $[Q]$ are both sparse matrices. Solving the eigenvalue equation yields the effective indices of guided modes $n_{eff} \equiv \beta/k_0$, where $k_0 = 2\pi/\lambda$ is the wave vector in free space. The modal birefringence of the fiber is then obtained by $B \equiv |n^x_{eff} - n^y_{eff}|$, where n^x_{eff} and n^y_{eff} are effective indices of the x- and y-polarized fundamental modes, respectively. In order to model infinite PCF with two-dimensional-finite-geometry (i.e., to enclose the computational domain without affecting the numerical solution), it is necessary to use anisotropic perfectly matched layers (PMLs) which are placed in the contact with the outer most boundary.

Firstly, a comparison of the difference on birefringence between elliptical air holes PCFs with triangular and tetragonal lattice (see Fig. 1(a)) has been performed, taking into account in the wavelength range between 0.8 µm and 2.4 µm. In the simulation models, each elliptical air hole forms the cladding with a pitch (center to center distance between the holes), Λ_x and Λ_y along x-axis and y-axis, respectively. As seen in Figs. 1(a), 2(a) and 2(b) denote the length of the elliptical air holes along x (minor axes) and y (major axis) directions, respectively, and the elliptical ratio is set $a/b = 0.3$. The core is formed by the omission of one elliptical air hole in the center of

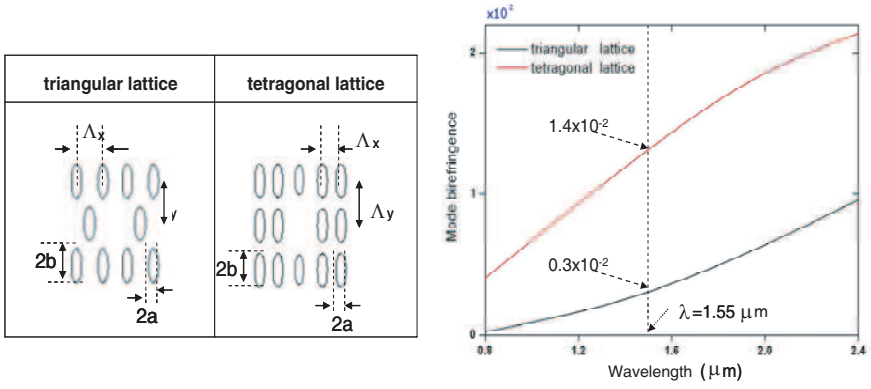

(a) (b)

Figure 1. (a) Schematic diagram of the geometric arrangement of elliptical air holes PCFs with triangular and tetragonal lattice. (b) Comparison of the difference on birefringence between elliptical air holes PCFs with triangular and tetragonal lattice.

this structure. The refractive index of the background silica is set as $n = 1.45$ and the air-holes is set to be 1 throughout the simulations. In this case, we set the number of the elliptical air hole layers is assumed to be $N = 4$ (i.e., four-ring elliptical air holes), $a = 0.27\,\mu\text{m}$, $b = 0.9\,\mu\text{m}$, $\Lambda_x = 3.1a$ and $\Lambda_y = 2.4a$, respectively.

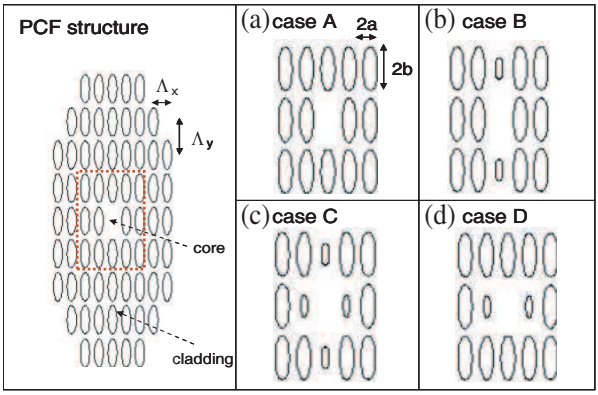

Figure 2. Cross section of four types (case A–D) proposed PCF structures.

In Fig. 1(b), the simulation results show that the mode birefringence formed by the PCF cladding with tetragonal lattice are larger than that of triangular lattice one. The mode birefringence for the tetragonal lattice case operated at the excitation wavelength of $\lambda = 1550\,\text{nm}$ can be achieved at a magnitude of 1.4×10^{-2} which is more than four times as large when compared to the triangular lattice case (0.3×10^{-2}). This is attributed to the index difference between the two orthogonal polarization states of tetragonal lattice case is larger than that of triangular lattice case. Thus, in this paper we focus on the PCF structure employing elliptical air holes in fiber cladding with tetragonal lattice in fused silica to compare their properties on mode birefringence and confinement loss.

Firstly, four patterns of PCF, which are composed by different sizes of elliptical air holes near the core and a cladding which consist of elliptical air holes with tetragonal lattice in fused silica, are analyzed for comparison, as shown in Figs. 2(a)–(d). For convenience, we name the corresponding fibers as case A [all of the sizes of elliptical air holes are the same, see Fig. 2(a)], case B [the same as case A, but air holes above and below the core are half the size of others, see Fig. 2(b)], case C [the same as case A, but four air holes near the core are half the size of others, see Fig. 2(c)], and case D [the same as case A, but left and right air holes near the core are half the size of others, see

Fig. 2(d)], respectively.

Figure 3 shows the Effective indexes as a function of wavelengths of four cases (A–D) of PCFs with the parameters Λ_x=2.04a, $\Lambda_y = 2.04b$, $a/b = 0.3$, $a = 0.27\,\mu$m, $b = 0.9\,\mu$m for the x-polarized and y-polarized light waves propagating in the z-direction.

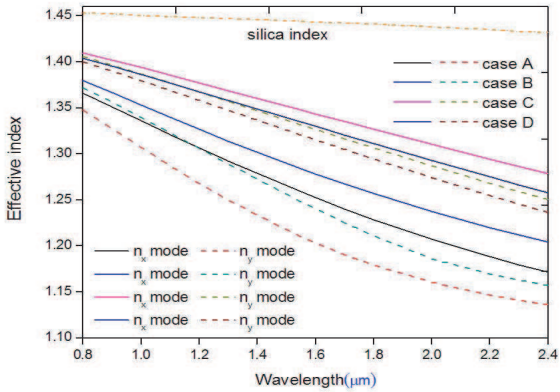

Figure 3. Effective indexes as a function of wavelengths of four cases (A–D) of PCFs with the parameters $\Lambda_x = 2.04a$, $\Lambda_y = 2.04b$, $a/b = 0.3$, $a = 0.27\,\mu$m, $b = 0.9\,\mu$m.

The background index of silica is calculated through the Sellmeier equation [9]. It is expressed as

$$n^2(\lambda) = 1 + \frac{B_1\lambda^2}{\lambda^2 - C_1} + \frac{B_2\lambda^2}{\lambda^2 - C_2} + \frac{B_3\lambda^2}{\lambda^2 - C_3}, \tag{1}$$

where λ is the wavelength of incident light and n is the refractive index of silica. The coefficient of Sellmeier "B" is the oscillator strengths of transitions, and "C" is the squares of the respective transition energies (as photon wavelengths). We set $B_1 = 0.96166300$, $B_1 = 0.407942600$, $B_1 = 0.897479400$, $C_1 = 0.00467914826$, $C_2 = 0.0135120631$ and $C_3 = 97.9340025$ for fused silica in our calculations, respectively. It can be seen from Fig. 3 that case A possesses larger difference of effective indexes between x-polarized and y-polarized than other three cases. For all cases, a difference between the effective indexes for different polarizations is observed and the effective indexes decreases with increasing wavelength. It is worthy to note that the difference of effective indexes of x-polarized are larger than y-polarized light waves due to the effective area of elliptical air hole along x axes (minor axes) is smaller than that of y axes (major axes).

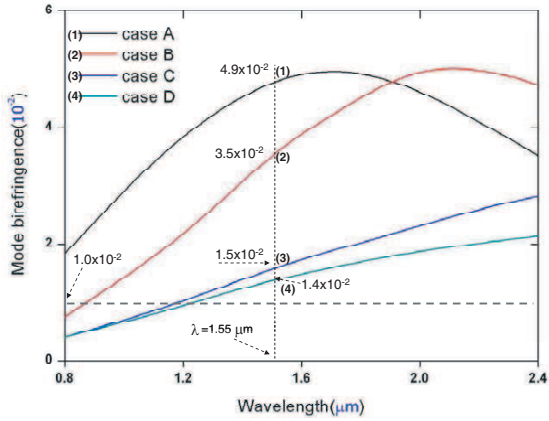

Figure 4. Birefringence as function of wavelengths for the four cases of PCFs with the parameters $\Lambda_x = 2.04a$, $\Lambda_y = 2.04b$, $a/b = 0.3$, $a = 0.27\,\mu\text{m}$, $b = 0.9\,\mu\text{m}$.

Figure 4 shows the birefringence as function of wavelengths for the four cases of PCFs with the parameters $\Lambda_x = 2.04a$, $\Lambda_y = 2.4b$, $a/b = 0.3$, $a = 0.27\,\mu\text{m}$, $b = 0.9\,\mu\text{m}$, at excitation wavelength $\lambda = 1550\,\text{nm}$. It can be clearly seen in Fig. 4 that the birefringence is sensitive to the variation of wavelengths, and the birefringence in cases A are also higher than those of case B–D. It is worthy to note that high birefringence above the order of 10^{-2} can be achieved from the proposed case A and B cases in a broad range of wavelengths ($0.8\,\mu\text{m} < \lambda < 2.4\,\mu\text{m}$). The corresponding maximum birefringence at excitation wavelength $\lambda = 1550\,\text{nm}$ for case A is 4.9×10^{-2}, for case B is 3.5×10^{-2}, for case C is 1.5×10^{-2} and for case D is 1.4×10^{-2}. To illustrate the field profile of case A–D, the corresponding fundamental mode at excitation wavelength $\lambda = 1.55\,\mu\text{m}$ are shown in Fig. 5. The simulated results of the y- and x-polarized mode are strongly bounded in the high index core region, respectively. It is evident in Fig. 5 that the field intensity of the x-polarized mode is stronger than that of the y polarized due to the x-polarized states have the lower air filling fraction than the y polarized states. It implies that the asymmetry in elliptical air hole PCFs with tetragonal lattice in fused silica is one of the key factors in determining the localization extent of the transverse mode. Another significant result from Fig. 5 is that the asymmetric core shape can influence the polarization mode in PCFs and can split the fields extended far beyond the core-cladding interface. It is worthy to confirm that if the large birefringence is desired, the parameters in

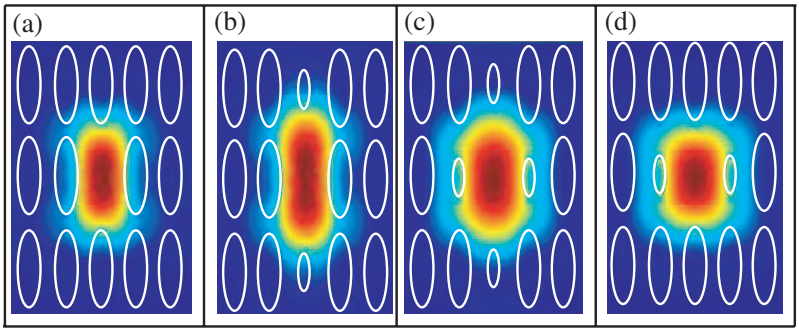

Figure 5. Corresponding fundamental mode of case A–D shown in Fig. 4 at excitation wavelength $\lambda = 1.55\,\mu\text{m}$.

PCFs are limited by the requirement for mode profiles, which contain higher fields intensity in the core region.

The asymmetry as well as the leakage (or loss) in elliptical air hole PCFs due to the interruption of the lattice are evident. The field confinement and its decay rate play a fundamental role in the leakage properties. They depend on the air hole diameter, on their pitch and on the number of rings. In practice, 6 to 10 rings of air holes are often needed to reduce the confinement loss to an acceptable level. For the sake of accuracy, we use 14 rings in this case. The influence of four cases of PCF on the birefringence stability is also significantly, which is illustrated in Fig. 6. It can be clearly seen from the Fig. 6 that the birefringence of cases A–D are stable and case A (near 5×10^{-2}) is higher than others, even in the case of the numbers of rings $N = 14$.

The FEM with PMLs which placed before the outer boundary can be use to calculate the confinement loss of PCFs. The confinement loss can be deduced from the imaginary part of the complex effective mode index and determined according to the following formulation:

$$\text{Confinement loss} = \frac{2 \times 10^{10}}{\ln 10} \frac{2\pi}{\lambda} \text{Im}[n^i_{eff}]\ \text{dBm/km} \quad (i = x, y) \qquad (2)$$

where $\text{Im}[n^i_{eff}]$ is the imaginary part of the effective index of the guided mode. Fig. 7 shows the confinement loss as a function of wavelength of four cases with fixed parameters, $\Lambda_x = 2.04a$, $\Lambda_y = 2.04b$, $a/b = 0.3$, $a = 0.27\,\mu\text{m}$, $b = 0.9\,\mu\text{m}$, at excitation wavelength $\lambda = 1550\,\text{nm}$ and the number of rings $N = 4$. It can be seen in Fig. 7, the case A and B structures display more confinement loss (0.04 dB/km and 0.021 dB/km, respectively), whereas case C and D (0.007 dB/km and 0.002 dB/km, respectively) structures can reduce at least a magnitude

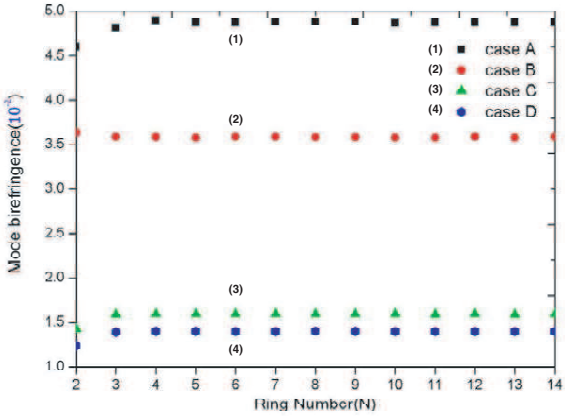

Figure 6. Mode birefringence of case A–D as a function of ring number with the same parameters used in Fig. 4. Where the excitation wavelength is $\lambda = 1.55\,\mu\text{m}$.

of one order of confinement loss than that of the case A and B. It is known that the confinement loss in a PCF decreases rapidly as more rings of air holes are introduced in the cladding. However, the confinement loss of case A structure (the number of rings $N = 4$) is about 0.04 dB/km, which is much lower than the value of about 490 dB/km (our calculated result from the model of Ref. [10]) obtained from a previous structure [10] with the small air holes array along x-axis when the air hole rings $N = 7$. To explain this phenomenon, the confinement field of our proposed case A–D structure is assigned to the PCF core, which is formed by the point defect and gives arise to more fields confined in the core region, thus the confinement loss decreases as more rings of holes are employed. In contrast, the small air holes array in the central part of Ref. [10] structure is a line defect, which demonstrates that most of the field leakage comes from the x-direction, and higher confinement loss is presented. In the same manner, the air holes near the PCF core of case A (all of elliptical air holes in PCF cladding are the same) are larger than those of other three cases (reduces some elliptical air holes near the core). Thus, the field leakage comes from the x- and y-directions are also larger than other cases, and higher confinement loss is presented.

Compared to the recent results of other approaches to achieve high birefringence and low loss PCFs, such as by adding many elliptical air holes in fiber core [6], by squeezed hexagonal lattice [4], by super-lattice structure PCFs [11], by decreasing stress factor [12], our proposed case A structure possesses both higher birefringence and lower loss in a

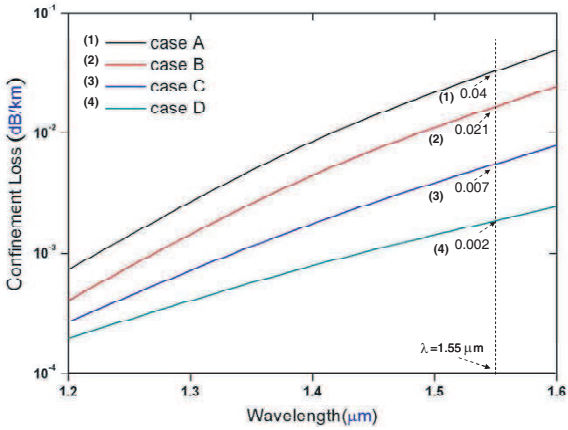

Figure 7. Confinement loss as a function of wavelengths of four cases PCFs with the same parameters used in Fig. 6.

broad range of wavelengths, and has the merit of ease procedures (all the same size of air holes) of fabrication.

Due to the performance of case A structure is superior to those of case B–C, now we focus on the structure of case A with different parameters of Λ_x and Λ_y to explore high birefringence and low confinement loss of PCF. The elliptical air holes in the fiber cladding are also arranged in a tetragonal lattice but with a shorter hole pitch. Fig. 8 shows the comparison of the birefringence obtained from case A as a function of wavelengths with fixing structure parameters $a = 0.27\,\mu\text{m}$, $b = 0.9\,\mu\text{m}$, and varying pitches (1) $\Lambda_x = 2.02a$, $\Lambda_y = 2.02b$, (2) $\Lambda_x = 2.04a$, $\Lambda_y = 2.04b$, (3) $\Lambda_x = 2.7a$, $\Lambda_y = 2.2b$ and (4) $\Lambda_x = 3.1a$, $\Lambda_y = 2.4b$, $a/b = 0.3$, at excitation wavelength $\lambda = 1550\,\text{nm}$ and the number of rings $N = 4$. It can be clearly seen that the birefringence is sensitive to the air hole spacing Λ_x and Λ_y as wavelength λ increases in the range of $[0.8, 2.4]\,\mu\text{m}$. The tendency of the birefringent curve in Fig. 8 is the same as those for the elliptical-hole PCFs [5] and squeezed hexagonal lattice PCF [4] with enlarging the lattice pitch along the x-axis as wavelength λ increases in the range of $[0.8, 1.6]\,\mu\text{m}$, we get the lower birefringent curves as the pitches Λ_x and Λ_y increasing. As shown in Fig. 8, the family curves of birefringence shift upward, corresponding to a decrement in the Λ_x and Λ_y values. Namely, the air hole spacing is also one of the key factors in determining the localization extent the transverse mode. The dispersion curves of birefringence increases over the wavelength in the range of $[0.8, 2.4]\,\mu\text{m}$. When Λ_x and

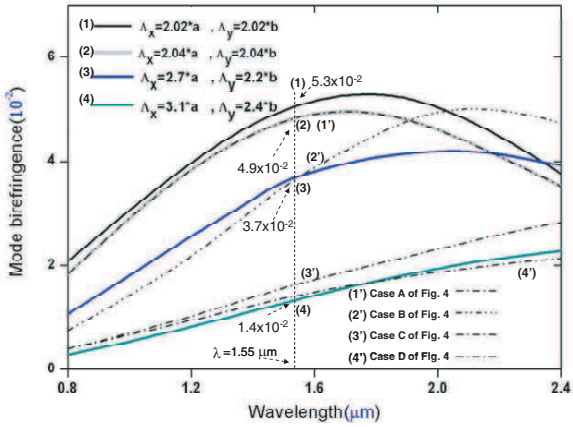

Figure 8. Comparison of the birefringence obtained from different pitches of case A as a function of wavelengths. Where the data of dashed lines [(1′)–(4′)] is obtained from case A–D of Fig. 4.

Λ_y are squeezed, while it decreases when Λ_x and Λ_y are enlarged, because squeezing Λ_x and Λ_y further increases the difference between the effective indices of y- and x-polarization modes, while enlarging Λ_x and Λ_y makes the difference less. To some extent this characteristic is similar to conventional elliptical core fibers [13, 14]. The corresponding wavelength $\lambda = 1.55\,\mu\text{m}$ with the birefringence reaches its maximum value $B = 5.3 \times 10^{-2}$ at $\Lambda_x = 2.02a$ and $\Lambda_y = 2.02b$ and minimum value $B = 1.4 \times 10^{-2}$ at $\Lambda_x = 3.1a$ and $\Lambda_y = 2.4b$, giving an enhancement of 3.9×10^{-2} by the effect of scaling air hole spacing along x- and y-axes. It may then be concluded that the birefringence can be increased by squeezing the hole spacing Λ_x and Λ_y along x- and y-axes. In order to compare the results of difference on birefringence with Fig. 4, we put the data of case A–D obtained from Fig. 4 with dashed lines [(1′)–(4′)] as indicted in Fig. 8. As can be seen from the comparison of solid and dashed lines in Fig. 8, we can learn that structures with smaller pitches for a fixed air hole size ratio exhibits higher birefringence. It is worthy to emphasize that high birefringence above the magnitude of 2×10^{-2} can be achieved from the proposed case A (with parameters $\Lambda_x < 2.04a$ and $\Lambda_y < 2.04b$) in a broad range of wavelengths ($0.8\,\mu\text{m} < \lambda < 2.4\,\mu\text{m}$), which is one order higher than those of case A and B shown in Fig. 4.

Although we have seen that the birefringence can be increased to a magnitude above 5×10^{-2}, the confinement loss still needs to be evaluated before one can conclude the fiber structure to be useful.

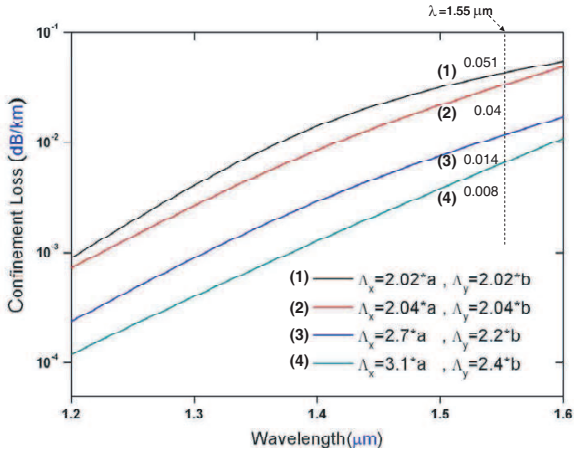

Figure 9. Comparison of the confinement loss of case A as a function of wavelength with different pitches and the same parameters used in Fig. 8.

Fig. 9 also shows the confinement loss of case A as a function of wavelength with different pitches and the same parameters used in Fig. 8. It can be seen in Fig. 9 that the confinement losses increases as the wavelength increases. The confinement loss is in the range of ~ 0.051 to 0.008 dB/km (can be obtained lower values when $N > 4$), indicating that the confinement loss can be tuned by the pitches along x- and y-axes, and its decay rate depend on the air-hole diameter and on the number of rings. If the PCF is required to have an acceptable confinement loss less than 0.1 dB/km, the birefringence will increase to a level above 0.001. Thus, there is a tradeoff between the confinement loss and the birefringence for an elliptical-hole with tetragonal lattice PCF like a structure of case A which indicating that the high mode birefringence and low confinement loss are maintained.

Figure 10 shows the ellipticity (a/b) dependence of birefringence of case A–D with fixed parameters: $\Lambda_x = 2.02a$, $\Lambda_y = 2.02b$, ring number $N = 4$ and excitation wavelength $\lambda = 1.55\,\mu$m. With the ellipticity a/b ranging from 0.15 to 0.45, the value of birefringence of case A exceeds a level of 3×10^{-5} and achieves a highest magnitude of 5.7×10^{-2} as $a/b = 0.25$. In additions, the value of birefringence of case B can be also reached a level of 3×10^{-5} as a/b ranging from 0.18 to 0.45. Turning to the value of birefringence of case C and D, the birefringence decreases as a/b ratio increases. From these results, hole ellipticity (a/b) is also a key point to enhance mode birefringence of elliptical air hole PCFs due to the difference of $n^x_{eff} - n^y_{eff}$ of case A

is larger than those of other cases.

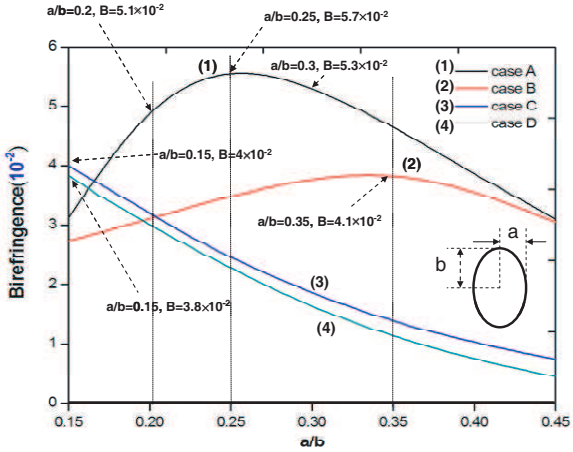

Figure 10. Birefringence of hole ellipticity (a/b) as a function of wavelengths with fixed parameters: $\Lambda_x = 2.02a$, $\Lambda_y = 2.02b$, ring number $N = 4$ and excitation wavelength $\lambda = 1.55\,\mu$m.

Even though the present study is purely numerical, at the end of this paper we would like to briefly comment on the possible fabrication issues for the proposed fiber structure. For current PCFs with elliptical holes, typically there is considerable variation in precise hole size and shape [12]. The holes may be particularly susceptible to changes in shape due to collapse and the surface tension may also tend to pull elliptic holes into circular ones. It seems that up to date one of the most promising fabrication methods that can overcome these problems may be the new multi-step process of forming preforms [15]. In additions, PCFs with elliptical holes were experimentally realized in 2004 [16], With the appearance of new methods for fabricating PCFs, such as performs drilling, solgel casting, and tapering [4, 16, 17], it is possible for us to draw PCFs with our proposed structures.

3. CONCLUSION

In conclusion, we numerically compare the mode birefringence and confinement loss with four patterns (case A–D) of index-guiding PCF using the FEM. These PCFs are composed of a solid silica core surrounded by four cases of different size of elliptical air holes and a cladding which consist of the same elliptical air holes. The maximal modal birefringence and lowest confinement loss of our proposed case A

structure at the excitation wavelength of $\lambda = 1550\,\text{nm}$ can be achieved at a magnitude of 5.3×10^{-2} and less than $0.051\,\text{dB/km}$ with only four rings of air holes in fiber cladding, respectively. There is a tradeoff between the confinement loss and the birefringence for an elliptical-hole PCF like a structure of case A which indicating that the high mode birefringence and low confinement loss are maintained. Moreover, it is worthy to note that high birefringence above the order of 10^{-2} can be achieved from the proposed case A and B in a broad range of wavelengths ($0.8\,\mu\text{m} < \lambda < 2.4\,\mu\text{m}$). Moreover, with the ellipticity a/b ranging from 0.15 to 0.45, the value of birefringence of case A exceeds a level of 3×10^{-5} and achieves a highest magnitude of 5.7×10^{-2} as $a/b = 0.25$. The merit of our designed PCFs is that the birefringence and confinement loss can be easily controlled by turning the pitch (hole to hole spacing) of elliptical air holes with tetragonal lattice in PCF cladding. Our simulation results provide valuable insight into realization of PCF with even appreciable birefringence than those demonstrated previously in literature.

ACKNOWLEDGMENT

Y.-F. Chau acknowledges the financial support from the National Science Council of the Republic of China (Taiwan) under Contract No. NSC 96-2112-M-231-001-MY3 and NSC-98-2120-M-002-004-.

REFERENCES

1. Shen, G.-F., X.-M. Zhang, H. Chi, and X.-F. Jin, "Microwave/millimeter-wave generation using multi-wavelength photonic crystal fiber brillouin laser," *Progress In Electromagnetics Research*, Vol. 80, 307–320, 2008.
2. Nozhat, N. and N. Granpayeh, "Specialty fibers designed by photonic crystals," *Progress In Electromagnetics Research*, Vol. 99, 225–244, 2009.
3. Guenneau, S., A. Nicolet, F. Zolla, and S. Lasquellec, "Numerical and theoretical study of photonic crystal fibers," *Progress In Electromagnetics Research*, Vol. 41, 271–305, 2003.
4. Yue, Y., G. Kai, Z. Wang, T. Sun, L. Jin, Y. Lu, C. Zhang, J. Liu, Y. Li, Y. Liu, S. Yuan, and X. Dong, "Highly birefringent elliptical-hole photonic crystal fiber with squeezed hexagonal lattice," *Opt. Lett.*, Vol. 32, 469–471, 2007.
5. Steel, M. J. and R. M. Osgood, Jr., "Elliptical hole photonic crystal fibers," *Opt. Lett.*, Vol. 26, 229–231, 2001.

6. Chen, D. and L. Shen, "Ultrahigh birefringent photonic crystal fiber with ultralow confinement loss," *IEEE Photon. Technol. Lett.*, Vol. 19, 185–187, 2007.
7. Chau, Y. F., H. H. Yeh, and D. P. Tsai, "Significantly enhanced birefringence of photonic crystal fiber using rotational binary unit cell of elliptical-hole with squeezed triangular lattice," *Jpn. J. Appl. Phys.*, Vol. 46, 1048–1051, 2007.
8. Jin, J., *The Finite Element Method in Electromagnetics*, John Wiley and Sons, Inc., New York, 2002.
9. Bach, H. and N. Neuroth, *The Properties of Optical Glass*, Springer, Heidelberg, 1995.
10. Ortigosa-Blanch, A., J. C. Knight, W. J. Wadsworth, J. Arriaga, B. J. Mangan, T. A. Birks, and P. S. J. Russell, "Highly birefringent photonic crystal fibers," *Opt. Lett.*, Vol. 25, 1325–1327, 2000.
11. Chen, D., M.-L. Vincent Tse, and H.-Y. Tam, "Super-lattice structure photonic crystal fiber," *Progress In Electromagnetics Research M*, Vol. 11, 53–64, 2010.
12. Liu, Y. C. and Y. Lai, "Optical birefringence and polarization dependent loss of square- and rectangular-lattice holey fibers with elliptical air holes: Numerical analysis," *Opt. Express*, Vol. 13, 225–235, 2005.
13. Kim, B. Y., J. N. Blake, S. Y. Huang, and H. J. Shaw, "Use of highly elliptical core fibers for two-mode fiber devices," *Opt. Lett.*, Vol. 12, 729–731, 1987.
14. Blake, J. N., S. Y. Huang, B. Y. Kim, and H. J. Shaw, "Strain effects on highly elliptical core two-mode fibers," *Opt. Lett.*, Vol. 12, 732–734, 1987.
15. Falkenstein, P., C. D. Merritt, and B. L. Justus, "Fused performs for the fabrication of photonic crystal fibers," *Opt. Lett.*, Vol. 29, 1858–1860, 2004.
16. Issa, N. A., M. A. V. Eijkelenborg, and M. Fellew, "Fabrication and study of microstructured optical fibers with elliptical holes," *Opt. Lett.*, Vol. 29, 1336–1338, 2004.
17. Domachuk, P., A. Chapman, E. Mägi, M. J. Steel, H. C. Nguyen, and B. J. Eggleton, "Transverse characterization of high air-fill fraction tapered photonic crystal fiber," *Appl. Opt.*, Vol. 44, 3885–3892, 2005.